

## Improving aeroelastic characteristics of helicopter rotor blades in forward flight

Hossam T. Badran<sup>\*1</sup>, Mohammad Tawfik<sup>2a</sup> and Hani M. Negm<sup>1b</sup>

<sup>1</sup>Aerospace Engineering Department, Cairo University, Giza 12511, Egypt

<sup>2</sup>Academy of Knowledge, Cairo 11765, Egypt

(Received December 25, 2017, Revised August 1, 2018, Accepted August 31, 2018)

**Abstract.** Flutter is a dangerous phenomenon encountered in flexible structures subjected to aerodynamic forces. This includes aircraft, helicopter blades, engine rotors, buildings and bridges. Flutter occurs as a result of interactions between aerodynamic, stiffness and inertia forces on a structure. The conventional method for designing a rotor blade to be free from flutter instability throughout the helicopter's flight regime is to design the blade so that the aerodynamic center (AC), elastic axis (EA) and center of gravity (CG) are coincident and located at the quarter-chord. While this assures freedom from flutter, it adds constraints on rotor blade design which are not usually followed in fixed wing design. Periodic Structures have been in the focus of research for their useful characteristics and ability to attenuate vibration in frequency bands called "stop-bands". A periodic structure consists of cells which differ in material or geometry. As vibration waves travel along the structure and face the cell boundaries, some waves pass and some are reflected back, which may cause destructive interference with the succeeding waves. In this work, we analyze the flutter characteristics of a helicopter blades with a periodic change in their sandwich material using a finite element structural model. Results shows great improvements in the flutter forward speed of the rotating blade obtained by using periodic design and increasing the number of periodic cells.

**Keywords:** finite element; vibration; periodic structure; rotor; helicopter; aeroelastic; flutter

---

### 1. Introduction

Since a helicopter rotor blade can be treated as a rotating flexible beam, the classic methods of determining the structural dynamics of a beam can be used. The free vibrations in both bending and torsional modes and natural frequencies for the rotating blade need to be determined. We will review some methods of calculating the coupled and uncoupled torsional and bending natural frequencies and mode shapes. Yntema (1955) is a notable example in which beams of variable cross section, but linear with span, and different root end suspensions are analyzed in detail for an untwisted rotor blade in pure vertical (flapwise) bending. However, a rotor blade undergoes vertical, inplane (chordwise) and torsional (twisting) deformations as it rotates about the main rotor drive shaft and a beam theory that includes motion in more than one plane is needed for use

---

\*Corresponding author, Ph.D., E-mail: [htbadran@hotmail.com](mailto:htbadran@hotmail.com)

<sup>a</sup> Associate Professor, E-mail: [mohammad.tawfik@gmail.com](mailto:mohammad.tawfik@gmail.com)

<sup>b</sup> Professor, E-mail: [hnegm\\_cu@hotmail.com](mailto:hnegm_cu@hotmail.com)

in a flutter theory. Wood and Hilzinger (1963) developed the fully coupled equations of motion for aeroelastic response of rotor blades that is based on the superposition of separated harmonics of blade forced response. This method is an extension of the work done by Gerstenberger and Wood (1963) on the coupled equations of motion for flapwise and chordwise bending, which uses the method developed by for calculating the natural frequencies and mode shapes. Lee and Lin (1994) studied the vibration of non-uniform rotating beams by neglecting the Coriolis Effect. Yang and Tsao (1997) studied the vibration and stability of a pretwisted blade under nonconstant rotating speed. Pohit *et al.* (1999) investigated free out-of-plane vibration of a rotating beam with a nonlinear elastomeric constraint. Bazoune *et al.* (2001) used the finite element method to study the dynamic response of spinning tapered Timoshenko beams. Vibration of a rotating damped blade with an elastically restrained root was investigated by Lin *et al.* (2004). A comparison between Bernoulli-Euler and Timoshenko beam theories in the analysis of a composite rotating beam was performed by Jung *et al.* (2001), Chandiramani *et al.* (2003). Singh (1985) studied turbine blade reliability with random properties.

The finite element technique has been used by many investigators for the vibration analysis of beams of uniform cross-section. These investigations differ from one another in the nodal degrees of freedom used for deriving the elemental stiffness and mass matrices. McCalley (1963) derived the consistent mass and stiffness matrices for a beam by selecting the total deflection and total slope as nodal co-ordinates. Kapur (1966) took the bending deflection, shear deflection, bending slope and shear slope as nodal degrees of freedom, and derived the elemental matrices of beams with linearly varying inertia. Thomas and Abbas (1975) analyzed uniform Timoshenko beams by taking the total deflection, total slope, bending slope and the derivative of the bending slope as nodal degrees of freedom. Improved two-node Timoshenko beam elements are developed based upon Hamilton's principle. Cubic and quadratic Lagrangian polynomials are used for the transverse and rotational displacements respectively, Friedman and Kosmatka (1993) and Don *et al.* (2015). Chen *et al.* (2016) proposes an efficient approach for dynamic analysis of a rotating beam using the discrete singular convolution (DSC). This method accurately captures not only the low-order but also the high-order frequencies of the beam rotating at a high angular velocity in very short time, compared with the classical finite element method.

Carrera Unified Formulation (CUF) is used to perform flutter analyses of fixed and rotary wings. The finite element method is used to solve the governing equations that are derived, in a weak form, using the generalized Hamilton's Principle. These equations are written in terms of CUF "fundamental nuclei", which do not vary with the theory order (N) (Filippi and Carrera 2015). An aeroelastic analysis of bearingless rotors is investigated using large deflection beam theory in hover and forward flight. The sectional elastic constants of a composite flex beam, including the warping deformations, are determined from a refined cross-sectional finite element method (Lim and Lee 2009). A new finite element model based on the coupled displacement field and the tapering functions of the beam is formulated for transverse vibrations of rotating Timoshenko beams of equal strength (Yardimoglu 2010). Kee and Shin (2015) investigate the dynamic characteristics of rotating composite blades. An eighteen-node solid-shell finite element was used to model the blade structures. The equations of motion for the finite element model were derived by using Hamilton's principle, and the resulting nonlinear equilibrium equations were solved by applying Newton-Raphson method combined with load control. A rotating beam finite element in which the interpolating shape functions are obtained by satisfying the governing static homogenous differential equation of Euler-Bernoulli rotating beams is developed by Babu Gunda and Ganguli (2008).

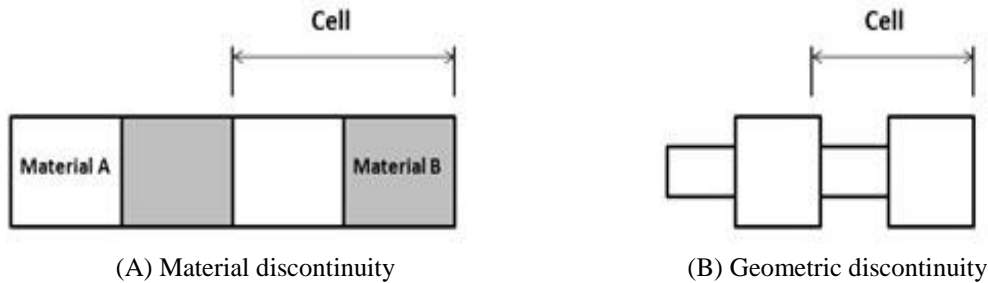


Fig. 1 Type of discontinuities

Loewy's 2-D unsteady aerodynamic theory (Loewy 1957), as amended by Hammond (1969), Jones and Rao (1970) provides a useful tool for examining blade flutter in hover. Additionally, Loewy showed how shed layers of vorticity affect Theodorsen's lift deficiency function (Theodorsen 1935), and influence the unsteady aerodynamic lift and moment equations. The present work will follow the analysis of Shipman and Wood, using Theodorsen's lift deficiency function. Carleton University's Rotorcraft Research Group is working on the development of an active rotor control system that incorporates a mechanism for helicopter blade pitch dynamic stiffness modulation at the root, the Active Pitch Link. Flutter oscillations of a typical section were controlled out over a range of airflow speeds (Nitzsche *et al.* 2015).

## 2. Periodic structures

A periodic structure consists fundamentally of a number of identical substructure components that are joined together to form a continuous structure. Recall what happens to Light wave as it travels through a boundary between two different media; part of the light wave refracts inside the water and the another part reflects back into air. The mechanical waves behave in a similar way and the reflected part of wave interferes with the incident wave (Mead 1996). There are two main types of discontinuities: (1) Geometric discontinuity and (2) Material discontinuity. Fig. 1 shows the basic idea of periodic structures and two different types of discontinuities. The transfer matrix approach, in general, is based on developing a relation between the two ends of a structural element. The real power of the transfer matrix approach comes when the structure can be divided into a set of substructures with a set of elements and nodes that are connected to another set on some fictitious boundary inside the structure (Mead and Parthan 1979).

Using the method of static condensation, the internal nodes / degrees of freedom of the substructure can be eliminated, thus reducing the size of the global matrices of the structure. When the set of equations of the substructure can be manipulated to collect the forces and displacements of one end of the substructure on one side of the equation, and relate them to those on the other end with a matrix relation, this matrix relation is called the transfer matrix of the structure. The transfer matrix of a substructure, other than being of reduced order, is then multiplied by that of the neighboring structure, in contrast with the superposition method that is used in conventional numerical techniques. Thus, the matrix system that describes the dynamics of the structure becomes of significantly smaller size. The transfer matrix method becomes of even more appealing features when the substructures can be selected in a manner that they are all identical, thus, calculating the transfer matrix for one substructure is sufficient to describe the dynamics of

the whole structure easily.

In this section, we review the research works performed in the area of wave propagation in periodic structures. Ungar (1966) derived an expression that describes the steady state vibration of an infinite beam uniformly supported on impedances. Later, Gupta (1970) presented an analysis for periodically-supported beams that introduced the concepts of the cell and the associated transfer matrix. He presented the propagation and attenuation parameter plots which form the foundation for further studies of one-dimensional periodic structures. Faulkner and Hong (1985) presented a study of general mono-coupled periodic systems. Their study analyzed the free vibration of spring-mass systems as well as point-supported beams using analytical and finite element methods. Mead and Yaman (1991) presented a study of the response of one-dimensional periodic structures subject to periodic loading. El-Din and Tawfik (2006) studied vibration attenuation in a periodic rotating Timoshenko beam using a finite element model.

An efficient numerical approach is proposed to study free and forced vibration of complex one-dimensional (1D) periodic structures (Zhou *et al.* 2015).

### 3. Mathematical modelling

A sandwiched rotating blade consists of 3 layers; a ceramic with rigid foam sandwiched between two aluminum layers. All layers are supposed to be perfectly bonded, under in plane-stress state, and having the same transverse displacement. The deformation of the face sheets obeys Euler-Bernoulli theory, while that of the core obeys Timoshenko theory. We will define all the mechanical quantities such as displacements, strains and energies in terms of the transverse displacements ( $w$ ) and longitudinal displacements of the top and bottom layers ( $u_t$ ) and ( $u_b$ ), respectively as shown in Badran *et al.* (2017). The longitudinal displacements of the layers are linear, the top and bottom layers resist axial and bending loads only, and the core layer resists shear load in addition to axial and bending loads. All layers resist torsion and centrifugal loads.

### 4. Development of equations of motion

The dynamic equations of motion in this investigation are developed using Hamilton's principle (Reddy 2002):

$$\delta \Pi = \int_{t_1}^{t_2} (\delta T - \delta U + \delta W) dt = 0 \quad (1)$$

By introducing and taking the first variation for strain energy, kinetic energy and external work, then integrating by parts with respect to time ( $t_1$  and  $t_2$  are arbitrary) we get the weak form of Hamilton's principle, which is used for deriving the finite element equations of the system. Since all layers bear axial, bending, torsion loads, and the core bears, in addition shear loads, then the total strain energy of the proposed model can be cast in this form:

$$U_i = \frac{1}{2} E^i A^i \int_0^L (u_i')^2 dx + \frac{1}{2} E^i I^i \int_0^L (w'')^2 dx + \frac{1}{2} G^i J^i \int_0^L (\varphi')^2 dx \quad (2)$$

$$U_c = \frac{1}{2} E^c A^c \int_0^L (u_c')^2 dx + \frac{1}{2} E^c I^c \int_0^L (\theta')^2 dx + \frac{1}{2} K_s G^c A^c \int_0^L (\gamma_{xz})^2 dx + \frac{1}{2} G^c J^c \int_0^L (\varphi')^2 dx \quad (3)$$

The bending and torsion strain energy due to rotation is given by

$$U_R = \frac{1}{2} (\rho^j A^j) \int_0^L f_c(x) (w')^2 dx + \frac{1}{2} (\rho^j I_o^j) \int_0^L f_c(x) (\varphi')^2 dx \quad (4)$$

The total kinetic energy for the proposed model can be cast in this form:

$$T_i = \frac{1}{2} \rho_i \int_0^L \left[ A_i (\dot{u}_i)^2 + I_i (\dot{w}')^2 + A_i (\dot{w})^2 \right] dx \quad (5)$$

$$T_c^p = \frac{1}{2} \rho_c \int_0^L \left[ A_c (\dot{u}_c)^2 + I_c (\dot{\theta}_c)^2 + A_c (\dot{w})^2 \right] dx \quad (6)$$

The external work applies on the proposed model is

$$W_t = \int_V \{q\}^T \{f_b\} dV + \int_A \{q\}^T \{f_s\} dA + \{q\}^T \{f_p\} \quad (7)$$

Where:  $\{f_b\}$ ,  $\{f_s\}$  and  $\{f_p\}$  and  $\{q\}$  are the external body, surface, point forces and nodal displacements respectively.

#### 4.1 Introducing centrifugal force $f_c(x)$

As shown in Fig. 2, the centrifugal force induced by rotation at station (x) within the  $i^{th}$  element, measured from its left end can be expressed as:

$$f_c(x) = \Omega^2 \int_x^L \rho A(\zeta) (R + \zeta) d\zeta \quad (8)$$

$$f_c(x) = \Omega^2 \left[ \int_x^{x_2^i} \rho A(\zeta) (R + \zeta) d\zeta + \sum_{j=i+1}^n \int_{x_1^j}^{x_2^j} \rho A(\zeta) (R + \zeta) d\zeta \right] \quad (9)$$

After making some mathematical manipulations, the centrifugal force can be cast in the form:

$$f_c(x) = f_o(x) + f_1(x) \quad (10)$$

Where:

$$f_o(x) = -\Omega^2 [\rho_i A_i (Rx + 0.5 x^2)]$$

$$f_1(x) = \Omega^2 \left[ \rho_i A_i (Rx_2^i + 0.5 x_2^{i2}) + \sum_{j=i+1}^n \rho_j A_j \left( (Rx_2^j + 0.5 x_2^{j2}) - (Rx_1^j + 0.5 x_1^{j2}) \right) \right]$$

The same procedure introduced above can be applied to the blade subjected to torsion by replacing the term  $(\rho A)$  by mass moment of inertia about elastic axis  $(\rho I_o)$  in Eq. (10).

Where,  $\rho_j A_j$  is average mass per unit length for the  $j^{th}$  element,  $\rho_i A_i$  is average mass per

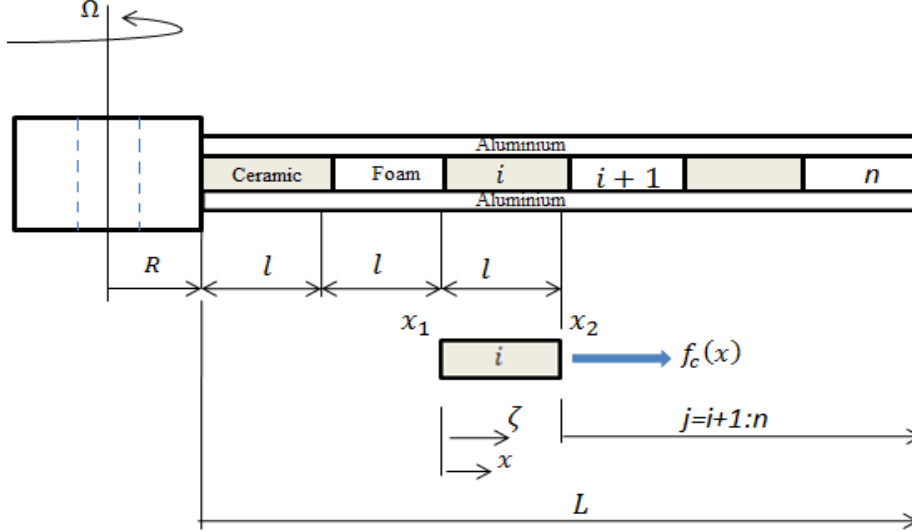


Fig. 2 Centrifugal force due to rotation

unit length for the  $i^{th}$  element, and  $R$  is hub radius.

#### 4.2 Variational formulation of system energy

By taking the first variation of the first integral of an element total strain energy with ceramic core we get:

$$\begin{aligned}
 \delta U_{to}^p = & \int_0^L \delta(u_t') B1(u_t') + \delta(u_b') B2(u_b') + \delta(w'') B3(w'') + \delta(u_t') (B4)(u_b') \\
 & + \delta(u_b') B4(u_t') + \delta(u_t') B5(w'') + \delta(w'') B5(u_t') + \delta(u_b') B6(w'') \\
 & + \delta(w'') B6(u_b') + \delta(u_t) B7 \delta(u_t) + \delta(u_b) B7(u_b) + \delta(w') B8(w') \quad (11) \\
 & - \delta(u_t) B9(u_b) - \delta(u_b) B9(u_t) - \delta(u_b) B10(w') - \delta(w') B10(u_b) \\
 & + \delta(u_t) B10(w') + \delta(w') B10(u_t)
 \end{aligned}$$

By taking the first variation of the first integral of an element total strain energy with foam core we get:

$$\begin{aligned}
 \delta U_{to}^f = & \int_0^L \delta(u_t') C1(u_t') + \delta(u_b') C2(u_b') + \delta(w'') C3(w'') + \delta(u_t') (C4)(u_b') + \delta(u_b') C4(u_t') \\
 & + \delta(u_t') C5(w'') + \delta(w'') C5(u_t') + \delta(u_b') C6(w'') + \delta(w'') C6(u_b') \\
 & + \delta(u_t) C7 \delta(u_t) + \delta(u_b) C7(u_b) + \delta(w') C8(w') - \delta(u_t) C9(u_b) \quad (12) \\
 & - \delta(u_b) C9(u_t) - \delta(u_b) C10(w') - \delta(w') C10(u_b) + \delta(u_t) C10(w') \\
 & + \delta(w') C10(u_t)
 \end{aligned}$$

Where B's and C's, are defined in Badran *et al.* (2017).

By taking the first variation of the first integral of element strain energy due to rotation we get:

$$\delta U_R = \int_0^L \delta(w') f_c(x) (w') dx \quad (13)$$

By taking the first variation of the first integral of element total kinetic energy with ceramic core we get:

$$\begin{aligned} \delta T_{to}^p = \int_0^L & \delta(\dot{u}_t) D1(\dot{u}_t) + \delta(\dot{u}_b) D2(\dot{u}_b) + \delta(\dot{w}) D3(\dot{w}) + \delta(\dot{u}_t) D4(\dot{u}_b) \\ & + \delta(\dot{u}_b) D4(\dot{u}_t) + \delta(\dot{u}_t) D5(\dot{w}) + \delta(\dot{w}) D5(\dot{u}_t) + \delta(\dot{u}_b) D6(\dot{w}) \\ & + \delta(\dot{w}) D6(\dot{u}_b) + \delta(\dot{w}) D7(\dot{w}) dx \end{aligned} \quad (14)$$

By taking the first variation of the first integral of element total kinetic energy with foam core we get:

$$\begin{aligned} \delta T_{to}^f = \int_0^L & \delta(\dot{u}_t) H1(\dot{u}_t) + \delta(\dot{u}_b) H2(\dot{u}_b) + \delta(\dot{w}') H3(\dot{w}') + \delta(\dot{u}_t) H4(\dot{u}_b) + \delta(\dot{u}_b) H4(\dot{u}_t) \\ & + \delta(\dot{u}_t) H5(\dot{w}') + \delta(\dot{w}') H5(\dot{u}_t) + \delta(\dot{u}_b) D6(\dot{w}') + \delta(\dot{w}') D6(\dot{u}_b) \\ & + \delta(\dot{w}') D7(\dot{w}') dx \end{aligned} \quad (15)$$

Where D's and H's are defined in (Badran *et al.* 2017).

By taking the first variation of the total external work done on the element we get:

$$\delta W_t = \int_V \{\delta q\}^T \{f_b\} dV + \int_A \{\delta q\}^T \{f_s\} dA + \{\delta q\}^T \{f_p\} \quad (16)$$

By substituting Eq.'s (11) to (16) into Eq. (1) we get the weak form of Hamilton's principle which we use in the finite element analysis.

## 5. Finite element formulation

The weak form of Hamilton's Principle stated in Eq. (1) will now be used to develop the finite element model of the suggested three-layer sandwich rotating blade with ceramic-foam core arranged side by side. Lagrange linear shape functions are used for axial displacement field  $u_t$ ,  $u_b$  which are  $C^0$ - type continuous, while Hermitian shape functions are used for transverse displacement  $w$ , which are  $C^1$ - type. This means that the deflection  $w$  and slope ( $\partial w / \partial x$ ) are continuous between two neighboring elements. The proposed model is a three-node finite beam element; each node has four mechanical degrees of freedom. The shape functions of the mechanical variables are similar to those in Badran (2008).

The element total stiffness matrix  $[K]$  will be derived with the help of Equations (11) and (12) for the different element with ceramic and foam cores after replacing the axial and transverse displacements by the assigned shape functions.

The stiffness matrix due to centrifugal acceleration can be derived using Eq. (13) as:

$$[K]_{c.f} = \int_{x_1^i}^{x_2^i} f_c(x) \delta_w^e T [N'_w]^T [N'_w] \delta_w^e \quad (17)$$

Where,  $[N'_w]$  and  $\delta_w^e$  are the first derivative of transverse displacement and shape function respectively which are similar to those in Badran (2008).

The element total mass matrix  $[M]$  will be derived with the help of Equations (14) and (15) for ceramic and foam cores after replacing the axial and transverse displacements by the assigned shape functions.  $[K]$ ,  $[K]_{c.f}$  and  $[M]$  are given in Badran (2018). Finally, the element nodal force vector can be derived using Eq. (16).

By substituting the mass, stiffness and force vector in Eq. (1), the equation of motion of a finite element can be written as:

$$[M]\{\ddot{q}\} + \left[ [K] + [K]_{c.f} \right] \{q\} = \{F\} \quad (18)$$

where, Coriolis effect are ignored, because the flexural and axial motion are uncoupled (Banerjee and Kennedy 2014).

## 6. Periodic analysis

Periodic structures can be modelled like any ordinary structure, however, studying the behaviour of one cell is sufficient to determine the stop and pass bands of the complete structure independent of the number of cells. In the present work, the frequency domain is classified into pass-bands, i.e. frequencies for which excited surface waves get through the periodic piezoelectric device, and stop-bands, i.e. frequencies which cannot pass through. Therefore, the piezoelectric device can be used for frequency filtering. There are two approaches for the analysis of the periodic characteristics of a beam: The forward approach and the reverse approach, as introduced in Badran *et al.* (2008b).

A code was developed for a periodic sandwich beam with a ceramic PZT (ignoring the piezoelectricity effect) and foam core, in order to study the effect of core structural periodicity on attenuating the vibration of beams. Fig. 3 shows the results obtained by the developed code for beams divided into different numbers of cells. The general specifications of the beam under study are mentioned in Badran (2008a). It is found that the response of the periodic sandwich beam is significantly improved through reduction of the vibration amplitudes at the positions of the stop bands.

It is found that the response of the periodic sandwich beam is significantly improved through reduction of the vibration amplitudes at the positions of the stop bands. Fig. 3 shows the effect of embedded periodic structures on the frequency response in a sandwich beam for a frequency range 0-2500 Hz. It is seen from the figure that the frequency response of the periodic sandwich beam has been significantly improved through reduction of the vibration amplitude at the position of stop bands.

By using the same MATLAB code, the normalized natural frequencies of rotating cantilever blade will be calculated. To validate the code, it was used to calculate the first and second dimensionless frequencies of flapwise motion of the rotating beam used in with these non-dimensional variables:  $\alpha = \sqrt{A L^2 / I_z}$ ,  $T = \sqrt{\rho A L^4 / E I_z}$ ,  $\delta = R/L$  and  $\gamma = T \Omega$ .

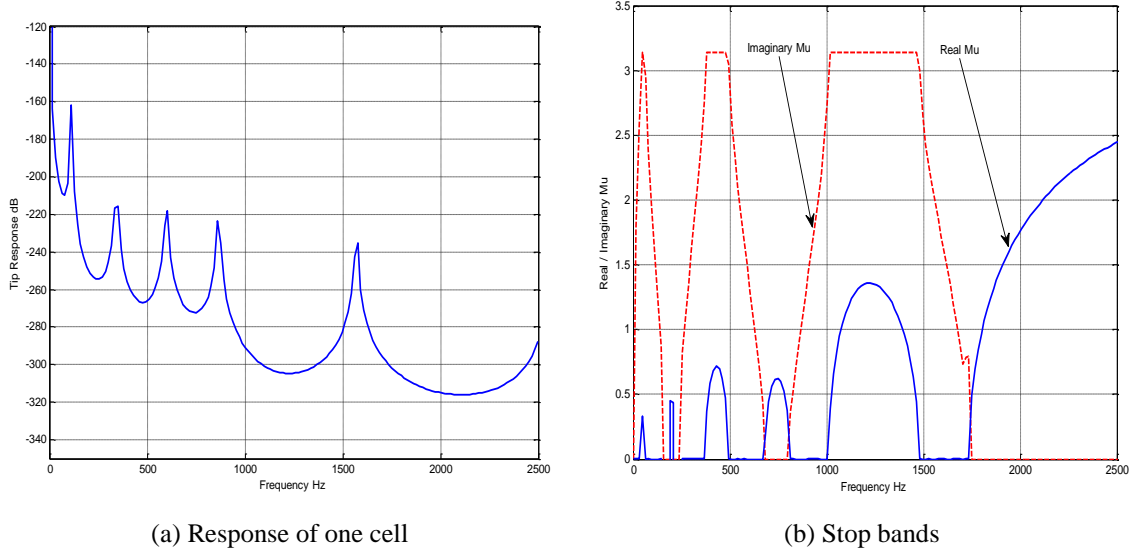


Fig. 3 Stop bands correspond to the drops in the frequency response

 Table 1 Dimensionless frequencies for the flapwise motion  $\alpha = 70$ 

$\gamma$	1 <sup>st</sup> natural frequency		2 <sup>nd</sup> natural frequency	
	Present work	Chung and Yoo (2002)	Present work	Chung and Yoo (2002)
0	3.5160	3.5160	22.0345	22.0345
1	3.6816	3.6816	22.1810	22.1810
2	4.1373	4.1373	22.6149	22.6149
3	4.7973	4.7973	23.3203	23.3203
4	5.5850	5.5850	24.2734	24.2733
5	6.4495	6.4495	25.4461	25.4461
Exact ( $\gamma = 0$ )	3.5160		22.0345	

Results are compared in Table 1. It is seen that the results have very good agreement.

## 7. Rotating blade flutter

The equations of motion are derived using energy methods by applying Hamilton's principle, which offers a convenient formulation for any number of discrete generalized or physical coordinates.

The assembled equation of motion of rotating blade has the form:

$$[M]\{\ddot{q}\} + [K]\{q\} = \{F\} \quad (19)$$

Where,  $\{q\}$  is the coordinate vector containing both the twisting and bending degrees of freedom:

$$\{q\}^T = \{w_1 \quad \theta_1 \quad \varphi_1, \dots \quad \dots \quad w_N \quad \theta_N \quad \varphi_N\}^T$$

For flutter analysis, a harmonic motion with oscillation frequency  $\omega$  is assumed, so the governing equation becomes:

$$(-\omega^2 [M] + [K])\{\bar{q}\} = \{\bar{F}\} \quad (20)$$

Where,  $\bar{q}$  is the amplitude of the deformation vector,  $\bar{F}$  is the amplitude of the load vector,  $[M]$  is the global mass matrix, and  $[K]$  is the global stiffness matrix. In Eq. (20) the right hand side is derived using an aerodynamic model, and the left hand side is derived using the structural model. The natural frequency ( $\omega$ ) occurs in a free vibration case where the system acts independent of the external forces.

### 7.1 Structural model

Double symmetry of the structure cross section leads to decoupling of the bending and torsional motions. The loss of cross sectional symmetry leads to a coupling effect between the bending and torsional motions due to an offset between the center of gravity and the shear center; a distance referred to as inertial eccentricity. The resulting equations of motion are inertially coupled, but elastically uncoupled.

The coupled elastic potential energy (U) is given as:

$$U = \frac{1}{2} EI \int_0^L (w'')^2 dy + \frac{1}{2} GJ \int_0^L (\varphi')^2 dy \quad (21)$$

The coupled kinetic energy (T) is given as:

$$T = \frac{1}{2} \int_{\text{chord}} (\dot{h})^2 dm \quad (22)$$

By referring to (Badran *et al.* 2017),  $h = -w - em \alpha$

Substituting (h) in Eq. (22) it can be shown that, (Guertin 2012)

$$T = \frac{1}{2} (\mu) \int_0^L (\dot{w})^2 dx + \frac{1}{2} (2 S_\alpha) \int_0^L (\dot{w})(\dot{\theta}) dx + \frac{1}{2} (I_\alpha) \int_0^L (\dot{\theta})^2 dx \quad (23)$$

By calculating the potential and kinetic energies of the structural model and applying Hamilton's principle, then using finite elements having two-nodes and three degrees of freedom per node (torsion, transverse displacement and rotation), we get the system of equations representing an eigen value problem. Solving these equations, we get the natural frequencies and mode shapes due to bending and torsion.

### 7.2 Aerodynamic model

The Theodorsen's 2-D thin airfoil theory will be used to evaluate the unsteady aerodynamic forces and moments per unit span  $L_i$  and  $M_i$  using thin aerofoil theory with a Theodorsen's lift deficiency function, (Bisplinghoff *et al.* 1996).

These can be cast in a matrix form as follows:

$$\begin{Bmatrix} L_i \\ M_i \end{Bmatrix} = \omega^2 \begin{bmatrix} L_{1i} & L_{2i} \\ M_{1i} & M_{2i} \end{bmatrix} \begin{Bmatrix} h_i \\ \alpha_i \end{Bmatrix} \quad (24)$$

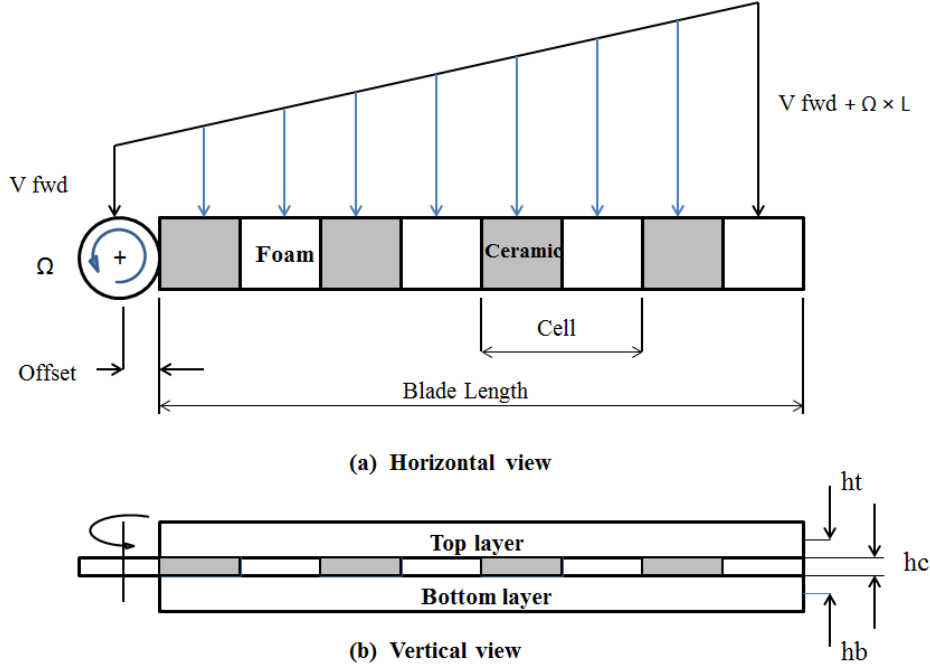


Fig. 4 Rotating periodic blade in forward flight

Where,  $L_{1i} = \pi \rho b_i^2 [L_h^i]$ ,  $L_{2i} = \pi \rho b_i^3 [L_\alpha^i - L_h^i (a + \frac{1}{2})]$ ,  $M_{1i} = \pi \rho b_i^3 [M_h^i - L_h^i (a + \frac{1}{2})]$ ,  $M_{2i} = \pi \rho b_i^4 [M_\alpha^i - (L_\alpha^i + M_h^i) (a + \frac{1}{2}) + L_h^i (a + \frac{1}{2})^2]$ ,  $\rho$ : air density,  $b_i$ : semi-chord,  $h$ : amplitude of the vertical displacement,  $\alpha_i$ : amplitude of the twisting angle,  $V_{fwd}$ : forward flight speed,  $L_h^i$ ,  $L_\alpha^i$ ,  $M_h^i$  and  $M_\alpha^i$  are aerodynamic lift and moment coefficients,  $k_r$ : reduced frequency and can be assumed as  $k_r = \omega b_i / (V_{fwd} + \Omega L)$  for forward flight and  $\omega$ : operating mode frequency as shown in Fig. 4.

Also according to the chosen flight condition, the lift deficiency function will be determined, which depends on modelling the wakes underneath the rotating blade. There are 3 different types of lift deficiency functions : (1) Theodorsen's lift deficiency function originally developed for fixed-wing aircraft where flow is subjected to small disturbances. (2) Loewy's lift deficiency function assumed that the rotor blade sections will encounter the shed wake from previous blades in case of hovering. (3) Shipman and Wood's lift deficiency function, which is analogous to Theodorsen, and Loewy's, but is modified to account for the helicopter's forward speed and the build-up and decay functions associated with the advancing blade.

The external virtual work done by the aerodynamic forces per unit span at an aerodynamic node can be written as follows:

$$F_i = \Delta y_i [\delta h_i \quad \delta \alpha_i] \begin{Bmatrix} L_i \\ M_i \end{Bmatrix} \quad (25)$$

Using three-node beam elements, the elastic axis deformation can be interpolated from the

deformation of the two end nodes by using first order polynomials for the torsional twist angle and third order polynomials for the transverse displacement as follows:

$$u_e = \begin{Bmatrix} h_i \\ \alpha_i \end{Bmatrix} = [\mathbf{N}]\{q\}_e \quad (26)$$

Where  $[\mathbf{N}]$ , is the shape function vector,  $\{q\}_e$  is the end nodes deformation vector in the wing local axes. Substituting Eq. (26) into Eq. (24) and then into Eq. (25) we get:

$$F_i = \omega^2 \{\delta q\}_e^T [\mathbf{N}]^T [\mathcal{L}_i] [\mathbf{N}]\{q\}_e \quad (27)$$

Where,  $[\mathcal{L}_i] = \Delta y_i \begin{bmatrix} L_{1i} & L_{2i} \\ M_{1i} & M_{2i} \end{bmatrix}$

The elemental unsteady aerodynamic matrix  $[A]$  can be obtained by summing all the external virtual work done at all the aerodynamic nodes at the middle of the structural element (Badran *et al.* 2017):

So, the equation of the dynamic system after assembling all matrices can be written as:

$$(-\omega^2 [[M] + [A]] + [K])\{\bar{q}\} = 0 \quad (28)$$

The flutter analysis can be performed using the familiar  $V - g$  method (Bisplinghoff, Ashley *et al.* 1996). The structural damping coefficient ( $g$ ) is introduced in the equations of motion, representing the amount of damping that must be added to the structure to attain neutral stability at the given velocity. Negative values of structural damping ( $g$ ) indicate that the structure is stable, while positive values indicate instability. Flutter occurs when the structural damping coefficient ( $g$ ) equals the actual damping of the structure, which is nearly zero, (Hollowell and Dugundji 1984). Substituting in Eq. (28), the following eigenvalue problem is obtained:

$$\left( [K]^{-1} ([M] + [A]) - \left( \frac{1 + gi}{\omega^2} \right) [I] \right) \{\bar{q}\} = 0 \quad (29)$$

The above equation can be solved as:

$$([K]^{-1} [[M] + [A]]) \{\bar{q}\} = \left( \left( \frac{1 + gi}{\omega^2} \right) [I] \right) \{\bar{q}\} \quad (30)$$

$$([K]^{-1} [[M] + [A]]) \{\bar{q}\} = (Z[I])\{\bar{q}\} \quad (31)$$

The above equation can be solved for the complex eigenvalues ( $Z$ ) for several values of the reduced frequency by equating both the imaginary and real parts on both sides then we can calculate the flutter frequency ( $\omega_f$ ), damping ( $g$ ) and flutter speed ( $U_f$ ) as follows:

$$\omega_f = \sqrt{\frac{1}{Z(Re)}}, \quad \eta = \frac{Z(Im)}{Z(Re)}, \quad U_f = \frac{\omega_f b}{k} \quad (32)$$

The values of ( $g$ ) and ( $\omega$ ) are plotted vs. ( $U_f$ ), and the  $\omega$  value at  $g = 0$  represents the flutter frequency ( $\omega_f$ )

Table 2 UH-60 Natural frequencies of hingless UH-60 blade

Frequency Mode no. (Hz)	Non-Rotating Blade		Rotating Blade $\Omega = 27.02$ rad/s	
	Finite Elements Present work	Assumed Modes (Rauchenstein Jr 2002)	Finite Elements Present work	Assumed Modes (Rauchenstein Jr 2002)
1 <sup>st</sup> bending	0.6995	0.6358	4.6687	4.717
2 <sup>nd</sup> bending	4.3837	3.9839	12.0143	11.187
1 <sup>st</sup> torsion	21.0303	20.0498	21.0528	20.505

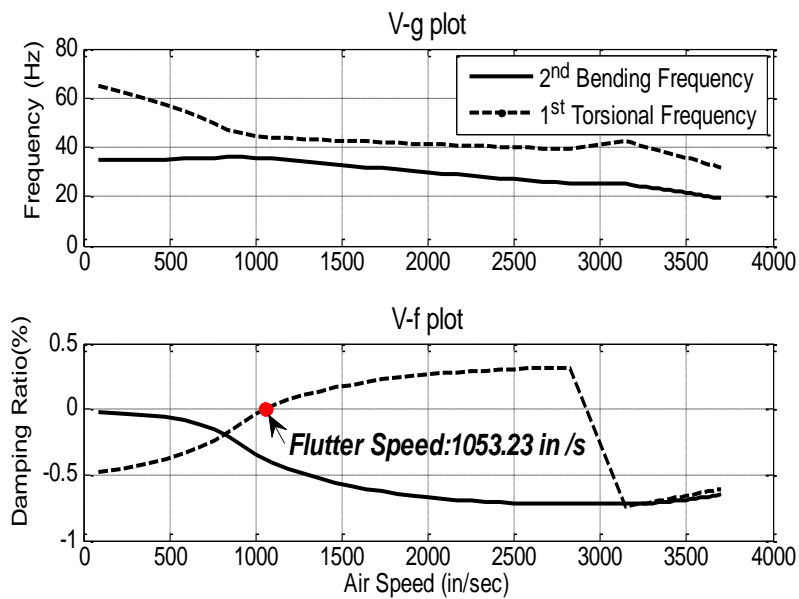


Fig. 5 UH-60 Wing flutter speed at constant rotating speed ( $\Omega = 27.02$  rad/s)

### 8. Flutter of helicopter rotor in forward flight numerical validation

A MATLAB code was developed for the periodic rotating blade. The finite element model consists of two models: A structural model, which is a geometric model of the blade, and an aerodynamic model, which calculates the unsteady aerodynamic loads acting on the rotating blade. The UH-60's blade is modelled as a uniform beam, incorporating the average geometric and inertial characteristics of the blade. However, for the demonstration analysis the UH-60 blade will be modified to make it "flutter susceptible" by moving the chord-wise position of the blade c.g aft while keeping its elastic axis at the quarter chord. Physically, the method of solution in this work is equivalent to locking the blade at the 90 -degree azimuth position and solving the flutter problems, similar to the fixed wing case with Theodorsen lift deficiency values.

Allowing radial velocity, and thus, the reduced frequency, to vary with the span as in the case of the tangential velocity of a rotor blade in forward flight.

The average characteristics of the UH-60 rotor blade are given in Norman *et al.* (2002). The rotating and non-rotating natural frequencies of the uniform blade model are

Table 3 UH-60 Rotor blade flutter speed

	Present work (finite elements)					Assumed modes
	No. of Elements					
	10	20	30	40	50	
Flutter Speed (fps)	1335	1139	1093	1067	1054	1054
Flutter frequency (rad/sec)	45.17	44.22	44.32	44.25	44.27	----

compared to those of the real blade given in Table 2.

It is seen that good agreement exists between the two sets of results giving confidence that the uniform beam model is adequate as a first order approximation of a real blade. With the mass matrix, stiffness matrix, natural frequencies and aerodynamic matrix calculated, the flutter analysis portion of the MATLAB program using finite elements is used to calculate the critical flutter forward speed for the blade at a given rotation speed and c.g location from the quarter chord to the 3/4 chord

Fig. 5 gives plots for the UH-60 rotor blades frequencies and damping ratios with the air speed, and the corresponding flutter speed at c.g. offset 72.5%. It is seen that the first torsional mode is the one that turns unstable.

Table 3 gives the calculated flutter speed and frequency for the UH-60 rotor blade using different numbers of finite elements, and compares them with those of Rauchenstein Jr. (2002). It is seen that dividing the rotor blade into 50 finite elements gives very good accuracy. By introducing the rotor flutter speed in forward flight and calculating the rotor tip speed then the maximum forward velocity is found to be  $V_{fwd} = 329$  fps (194.9 knots), which is the same value used in Rauchenstein Jr. (2002).

## 9. The proposed periodic rotating blade model

We will choose the dimensions of the rotor under investigation so as to have the same aspect ratio of the UH-60 Black Hawk helicopter main rotor as follows (Badran 2018): Rotor radius = 6 m , Chord = 0.39 m , blade thickness = 10% chord , blade aspect ratio = 14.79. The properties of Aluminum are: Density  $\rho = 2770 \text{ Kg/m}^3$ , Modulus of Elasticity  $E = 71 \times 10^9 \text{ N/m}^2$  and Modulus of rigidity  $G = 27.3 \times 10^9 \text{ N/m}^2$ . The material properties of Ceramic PZT are:  $\rho = 7750 \text{ Kg/m}^3$ ,  $E = 70.8 \times 10^9 \text{ N/m}^2$  and  $G = 23 \times 10^9 \text{ N/m}^2$ . The material properties for Foam are:  $\rho = 75 \text{ Kg/m}^3$ ,  $E = 73 \times 10^6 \text{ N/m}^2$  and  $G = 26 \times 10^6 \text{ N/m}^2$ . The rotation speed  $\Omega = 20 \text{ rad/s}$ .

Now we study the effect of periodic design on the flutter forward speed of a helicopter rotor made of aluminum of three layers, top, core and bottom. In order to make a fair comparison between the solid and periodic core models we use the same outer dimensions, total mass and flight conditions.

### 9.1 The flutter speed of solid core rotating blade

Fig. 6 shows the flutter forward speed of the proposed solid core blade at altitude 1000 m. It is that the flutter speed of the solid core rotor is 158.6 m/s.

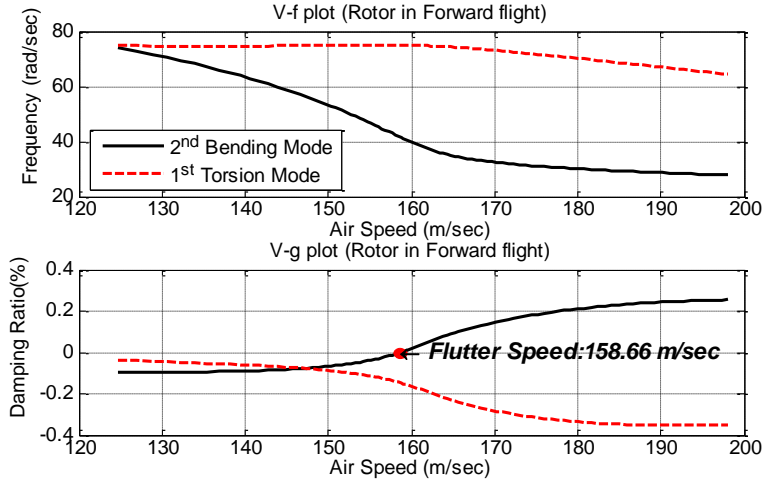


Fig. 6 Flutter speed of the rotating solid blade

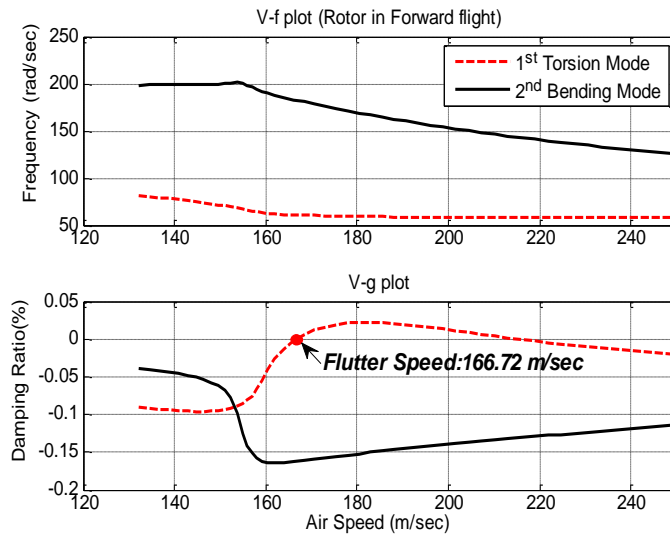


Fig. 7 Flutter speed of the rotating periodic core blade

### 9.2 Flutter speed of blade with periodic core

The proposed periodic core is a sandwich rotating blade with three layers: The top and bottom layers are made of aluminum, and the core is periodic PZT Ceramic-Foam side by side. We choose the main geometry of the periodic model to be similar to that of the solid model, with the same total thickness and length. In this case the mass is 243.9 Kg for the solid rotor. So we will change the thickness of the layers to have a thickness ratio ( $h_p/h_t$ ) of 0.5 and the lengths of the cells to have a cell length ratio ( $L_p/L_t$ ) of 0.54. These values reduce the mass of the proposed periodic core model to that of the solid model.

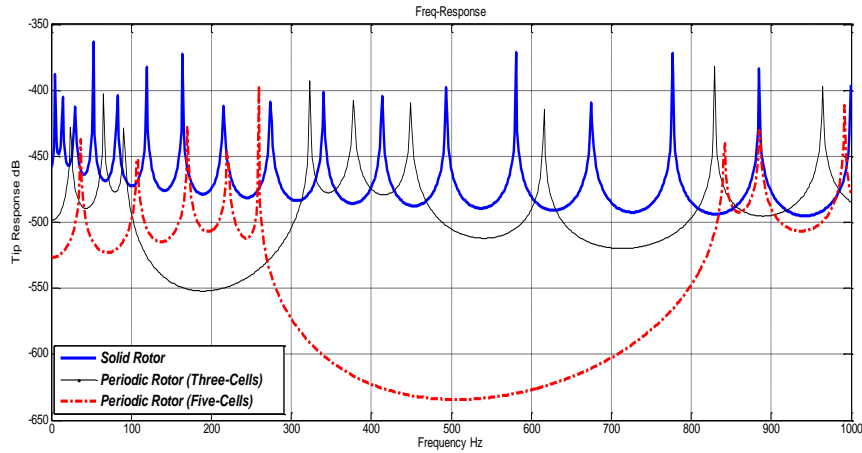


Fig. 8 Effect of number of cells on response of periodic rotor

Table 4 Variation of flutter frequency and flutter forward speed with the number of cells

Rotor Blade	Flutter Frequency (rad/s)	Flutter Speed (m/s)
Solid	41.5	158.6
Periodic (1 cell)	60.9	166.7
Periodic (2 cell)	252.5	880.5
Periodic (3 cell)	536.4	1079.0
Periodic (4 cell)	1261.8	1496.6
Periodic (5 cell)	1267.5	1561.3

Fig. 7 shows the flutter forward speed of the proposed periodic core rotating blade at the same altitude using one cell pair. The flutter speed of the sandwich periodic rotor is found to increase to 167 m/sec. This improvement can be explained by the existence of stop bands created by periodic design, which postpone the flutter frequency to a higher value.

Other calculations have been made to investigate the effect of increasing the number of cell pairs on the flutter forward speed of the rotor blade, keeping its outer dimensions, total mass, rotation speed and flight altitude unchanged.

Fig. 8 compares the frequency response of the solid rotor blade with that of the periodic blades having 3 and 5 cells pairs.

Table 4 gives the values of the flutter frequency and flutter forward speed of the rotor blade for different numbers of cell pairs. It is seen from the results that great improvements in the flutter forward speed can be obtained by increasing the number of cell pairs in the periodic design of the rotor blade. The reason for large jumps in the flutter forward speeds obtained for 2, 3 and 5 cells can be explained by the combined effect of the stop bands which shift the flutter frequencies to higher values and the fact that higher modes of vibration become the ones which turn unstable. The improvement is found to diminish quickly after using 5 cells. Naturally we should have used subsonic and supersonic aerodynamic theories when the blade tip speed increase to higher values. However, the obtained results using incompressible flow remain indicative of the flutter speed

improvement by the use of periodic design.

## 10. Conclusions

Aeroelastic performance of helicopter rotor blade structures is of extreme importance. A helicopter rotor blade must not experience flutter instability at all possible forward speeds. Periodic design of structures has proved to be useful in improving the dynamic performance in the absence of flow. A periodic structure is composed of repeated groups of cells of different material or geometry. This causes destructive interference between the waves travelling back and forth along the structure, and hence reduces its vibration level.

In this paper a periodic rotor blade design is suggested as a rotating beam composed of a core sandwiched between two aluminium face layers. The beam is divided into cells in which the core is made of piezo ceramic or foam patches in an alternate order. The flutter forward speed is calculated for such a periodic sandwich rotor using 3-node beam finite elements with shear, bending and torsional degree of freedom at each node in the structural analysis, and Theodorsen's 2-D thin aerofoil theory with a lift deficiency function for the unsteady aerodynamic analysis, assuming incompressible flow conditions. The blade flutter speed is calculated using the V-g method for a different number of pairs of periodic cells, and compared with that of the nonperiodic solid blade, keeping the outer dimensions, total mass (243.94 kg), rotation speed (20 rad/s) and flight altitude (1000 m) unchanged.

Results of the calculations show that good improvements in the flutter forward speed of the rotating blade can be obtained by using periodic design and increasing the number of periodic cells. This can be explained by the existence of the frequency stop bands created by the periodic design which shift the flutter frequencies to higher values. Also large jumps in the flutter forward speed are observed at certain numbers of cells pairs. This is caused by the fact that higher modes of blade vibration become the ones which turn unstable. Finally, the improvement is found to diminish after using a certain number of cells.

## References

- Babu Gunda, J. and Ganguli, R. (2008), "New rational interpolation functions for finite element analysis of rotating beams", *J. Mech. Sci.*, **50**(3), 578-588.
- Badran, H.T. (2008), "Vibration attenuation of periodic sandwich beams", M.Sc. Dissertation, Cairo University, Cairo.
- Badran, H.T. (2018), "Improving dynamic and aeroelastic performance of helicopter rotors using periodic design and piezo active control", Ph.D. Dissertation, Cairo University, Cairo.
- Badran, H.T., Tawfik, M. and Negm, H.M. (2017), "Improving wing aeroelastic characteristics using periodic design", *Adv. Aircraft Spacecraft Sci.*, **4**(4), 353-369.
- Banerjee, J. and Kennedy, D. (2014), "Dynamic stiffness method for inplane free vibration of rotating beams including Coriolis effects", *J. Sound Vib.*, **333**(26), 7299-7312.
- Bazoune, A., Khulief, Y.A., Stephen, N.G. and Mohiuddin, M.A. (2001), "Dynamic response of spinning tapered Timoshenko beams using modal reduction", *Finite Elem. Anal. Des.*, **37**(3), 199-219.
- Bisplinghoff, R., Ashley, H. and Halfman, R. (1996), *Aeroelasticity*, Dover Publication Inc., Mineola, New York, U.S.A.
- Chandiramani, N.K., Shete, C.D. and Librescu, L.I. (2003), "Vibration of higher-order-shearable pretwisted rotating composite blades", *J. Mech. Sci.*, **45**(12), 2017-2041.
- Chen, J., Ding, Y. and Ding, H. (2016), "An efficient approach for dynamic analysis of a rotating beam using

- the discrete singular convolution", *P. I. Mech. Eng. C. J. Mec.*, **230**(20), 3642-3654.
- Chung, J. and Yoo, H.H. (2002), "Dynamic analysis of a rotating cantilever beam by using the finite element method", *J. Sound Vib.*, **249**(1), 147-164.
- Don, M., Palmeri, A., Lombardo, M. and Cicirello, A. (2015), "An efficient two-node finite element formulation of multi-damaged beams including shear deformation and rotatory inertia", *Comput. Struct.*, **147**(C), 96-106.
- El-Din, M.A. and Tawfik, M. (2006), "Vibration attenuation in rotating beams with periodically distributed piezoelectric controllers", *Proceedings of the 13th International Congress on Sound and Vibration (ICSV'06)*, Vienna, Austria, July.
- Faulkner, M. and Hong, D. (1985), "Free vibrations of a mono-coupled periodic system", *J. Sound Vib.*, **99**(1), 29-42.
- Filippi, M. and Carrera, E. (2015), "Flutter analysis of fixed and rotary wings through a one-dimensional unified formulation", *Compos. Struct.*, **133**, 381-389.
- Friedman, Z. and Kosmatka, J.B. (1993), "An improved two-node Timoshenko beam finite element", *Comput. Struct.*, **47**(3), 473-481.
- Gerstenberger, W. and Wood, E.R. (1963), "Analysis of Helicopter Aeroelastic Characteristics in High-Speed Flight", *AIAA Journal*, **1**(10), 2366-2381.
- Guertin, M. (2012), "The application of finite element methods to aeroelastic lifting surface flutter", Ph.D. Dissertation, Rice University, Houston, Texas, U.S.A.
- Gupta, G.S. (1970), "Natural flexural waves and the normal modes of periodically-supported beams and plates", *J. Sound Vib.*, **13**(1), 89-101.
- Hammond, C.E. (1969), "Compressibility effects in helicopter rotor blade flutter", Ph.D. Dissertation, Georgia Institute of Technology, Atlanta, U.S.A.
- Hollowell, S.J. and Dugundji, J. (1984), "Aeroelastic flutter and divergence of stiffness coupled, graphite/epoxy cantilevered plates", *J. Aircraft*, **21**(1), 69-76.
- Jones, W. and Rao, B. (1970) "Compressibility effects on oscillating rotor blades in hovering flight", *AIAA Journal*, **8**(2), 321-329.
- Jung, S.N., Nagaraj, V.T. and Chopra, I. (2001), "Refined structural dynamics model for composite rotor blades", *AIAA Journal*, **39**(2), 339-348.
- Kapur, K.K. (1966), "Vibrations of a Timoshenko beam, using finite-element approach", *J. Acoustical Soc. America*, **40**(5), 1058-1063.
- Kee, Y.J. and Shin, S.J. (2015), "Structural dynamic modeling for rotating blades using three dimensional finite elements", *J. Mech. Sci. Technol.*, **29**(4), 1607-1618.
- Lee, S.Y. and Lin, S.M. (1994), "Bending vibrations of rotating nonuniform Timoshenko beams with an elastically restrained root", *J. Appl. Mech. T. ASME*, **61**(4), 949-955.
- Lim, I.G. and Lee, I. (2009), "Aeroelastic analysis bearingless rotors with a composite flexbeam", *Compos. Struct.*, **88**(4), 570-578.
- Lin, S.M., Lee, S.Y. and Wang, W.R. (2004), "Dynamic analysis of rotating damped beams with an elastically restrained root", *J. Mech. Sci.*, **46**(5), 673-693.
- Loewy, R.G. (1957), "A two-dimensional approximation to the unsteady aerodynamics of rotary wings", *J. Aeronaut. Sci.*, **24**(2), 81-92.
- McCalley, R. (1963), "Rotary inertia correction for mass matrices", Report DIG/SA: 63-73; General Electric Knolls Atomic Power Laboratory, Schenectady, New York, U.S.A.
- Mead, D. (1996), "Wave propagation in continuous periodic structures: Research contributions from Southampton, 1964-1995", *J. Sound Vib.*, **190**(3), 495-524.
- Mead, D. and Parthan, S. (1979), "Free wave propagation in two-dimensional periodic plates", *J. Sound Vib.*, **64**(3), 325-348.
- Mead, D. and Yaman, Y. (1991), "The response of infinite periodic beams to point harmonic forces: A flexural wave analysis", *J. Sound Vib.*, **144**(3), 507-529.
- Nitzsche, F., D'Assunção, D. and Junior, C.D.M. (2015), "Aeroelastic control of non-rotating and rotating wings using the dynamic stiffness modulation principle via piezoelectric actuators", *J. Intell. Mater. Syst.*

- Struct.*, **26**(13), 1656-1668.
- Norman, T.R., Shinoda, P.M., Kitaplioglu, C., Jacklin, S.A. and Sheikman, A. (2002), "Low-speed wind tunnel investigation of a full-scale UH-60 rotor system", National Aeronautics and Space Administration Moffett Field CA AMES Research Center, <https://apps.dtic.mil/dtic/tr/fulltext/u2/a480625.pdf>.
- Pohit, G., Mallik, A. and Venkatesan, C. (1999), "Free out-of-plane vibrations of a rotating beam with non-linear elastomeric constraints", *J. Sound Vib.*, **220**(1), 1-25.
- Rauchenstein Jr., W.J. (2002). "A 3D Theodorsen-based rotor blade flutter model using normal modes", Ph.D. Dissertation, Naval Postgraduate School, California, U.S.A.
- Reddy, J.N. (2002), *Energy Principles and Variational Methods in Applied Mechanics*, John Wiley and Sons, New York, U.S.A.
- Singh, M.P. (1985), "Turbine blade dynamics – A probabilistic approach", *Vib. Blades Bladed Disk Assemblies*, 41-48.
- Theodorsen, T. (1935), "General theory of aerodynamic instability and the mechanism of flutter", NACA-TR-496; Advisory Committee for Aeronautics, Langley, VA, U.S.A.
- Thomas, J. and Abbas, B. (1975), "Finite element model for dynamic analysis of Timoshenko beam", *J. Sound Vib.*, **41**(3), 291-299.
- Ungar, E.E. (1966), "Steady-state responses of one-dimensional periodic flexural systems", *J. Acoustical Soc. America*, **39**(5A), 887-894.
- Wood, E.R. and Hilzinger, K. (1963), "A method for determining the fully coupled aeroelastic response of helicopter rotor blades", *Proceedings of American Helicopter Society 19th Annual National Forum*, Washington, DC, May.
- Yang, S.M. and Tsao, S.M. (1997), "Dynamics of a pretwisted blade under nonconstant rotating speed", *Comput. Struct.*, **62**(4), 643-651.
- Yardimoglu, B. (2010), "A novel finite element model for vibration analysis of rotating tapered Timoshenko beam of equal strength", *Finite Elem. Anal. Des.*, **46**(10), 838-842.
- Yntema, R.T. (1955), "Simplified procedures and charts for the rapid estimation of bending frequencies of rotating beams", NACA-TN-3459; National Advisory Committee for Aeronautics. Langley Aeronautical Lab., VA, U.S.A.
- Zhou, C.W., Lainé, J.P., Ichchou, M.N. and Zine, A.M. (2015), "Wave finite element method based on reduced model for one-dimensional periodic structures", *J. Appl. Mech.*, **07**(02), 1550018.